

# SPRING-8 BEAM PERFORMANCE

## Developments and Upgrades of the Storage Ring and Linac

### Lower Emittance Optics for User Operation

To provide brilliant photons at the SPring-8 storage ring, new optics has been available for the user operation since May 9, 2013. The main parameters of new optics are listed in Table 1. The natural emittance of the new optics is reduced from 3.49 nm-rad to 2.41 nm-rad at 8 GeV by optimizing the quadrupole magnetic fields. Compared to the previous optics, SPECTRA [1] predicts that the new optics can provide 1.5-times higher brilliance and 1.25-times higher flux density for 10 keV photons with the SPring-8 standard undulator, and it was confirmed at the accelerator diagnostics beamline II (BL05SS) that the flux density of the new optics is 1.3-times higher than that of the previous ones (see Fig. 1).

Table 1. Main parameters of the new optics

	Previous Optics	New Optics
Beam energy	8 GeV	
Natural emittance	3.49 nm-rad	2.41 nm-rad
Energy spread $\sigma_E/E$	0.11%	
Tune ( $Q_x, Q_y$ )	(40.14, 19.35)	(41.14, 19.35)
Natural chromaticity ( $\xi_x, \xi_y$ )	(-88, -42)	(-117, -47)
( $\beta_x, \beta_y, D$ ) @ ID center	(22.5 m, 5.6 m, 0.11 m)	(31.2 m, 5.0 m, 0.15 m)

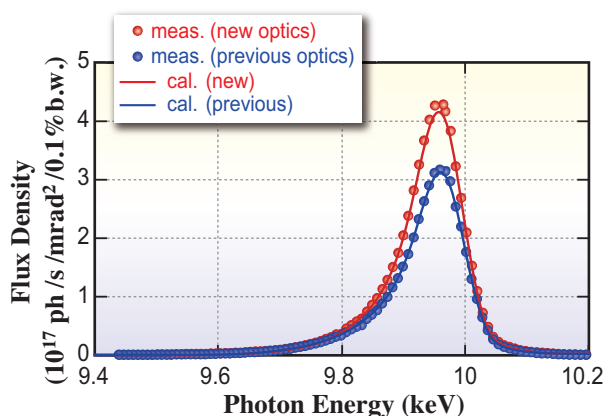


Fig. 1. Comparison of the photon flux density for the new and previous optics at diagnostics beamline II (BL05SS).

### Cure for Impact of Insertion Devices

In recent light source rings the top-up operation, where the electron beam is injected into the storage ring during user experiment, is essential for improving the integral brilliance and the strength stability of the light source. In the top-up operation the electron beam is injected with beam shutters for the photon beam opened and the gaps of insertion devices (ID) closed. Hence electron loss should be as small as possible for radiation safety and to prevent demagnetization of the magnet array of ID's.

Usually, the injected electron beam has a large horizontal oscillation amplitude being injected in the horizontal plane. This horizontal oscillation with is converted into a vertical oscillation by coupling of the betatron motion. Consequently, the beam is lost at a vertical obstacle that is narrower than the horizontal aperture. In particular, when the gap of the in-vacuum undulator is closed, the vertical aperture increases beam loss, becoming much smaller.

In the SPring-8 storage ring, linear betatron coupling is well suppressed by tuning the skew quadrupole magnets. Consequently, linear coupling scarcely affects the beam loss. However, higher-order coupling resonance is excited through the skew octupole magnetic field of ID07, which is a complex of eight Figure-8 undulators, and hence enhances beam loss. Figure 2 shows the operation point and the resonance lines of the betatron motion. As the oscillation amplitude grows, the betatron tune shifts to

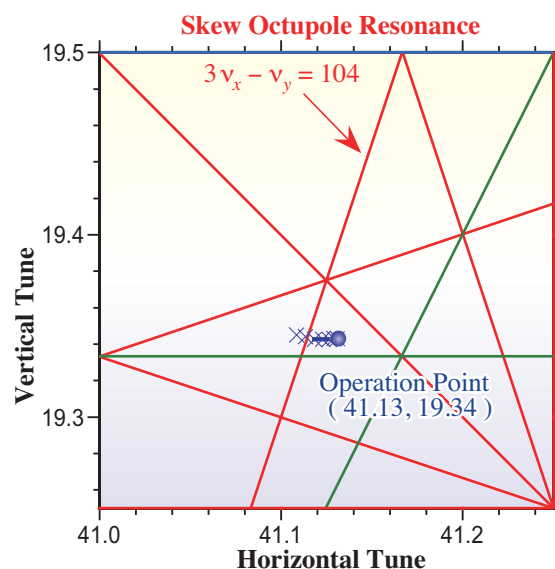


Fig. 2. Betatron tune and resonance lines in the tune diagram. Green and red lines denote the third and fourth order resonances, respectively.

the skew octupole resonance. Then electrons with a large amplitude like the injecting beam are lost due to the coupling resonance.

Octupole magnets installed to cancel the octupole magnetic field of ID07, improved the beam injection efficiency. Figure 3 shows the trend of the injection efficiency in user operation and the output current to the skew octupole magnets. The injection efficiency is recovered by exciting the octupole magnets.

Besides the skew octupole coupling resonance, the injection efficiency is degraded when the ID gaps are closed, especially that of ID19, which is a 25-m long in-vacuum undulator. Because the quadrupole magnetic field generated by ID19 shifts the betatron tune to approach the higher order coupling resonance according to the gap value, beam loss increases due to the resonance excitation. However, tuning the strength of neighboring quadrupole magnets can compensate for this tune shift and restore the injection efficiency. In user operations of the SPring-8 storage ring, the compensation for the effects of the insertion devices maintains the injection efficiency above 80%.

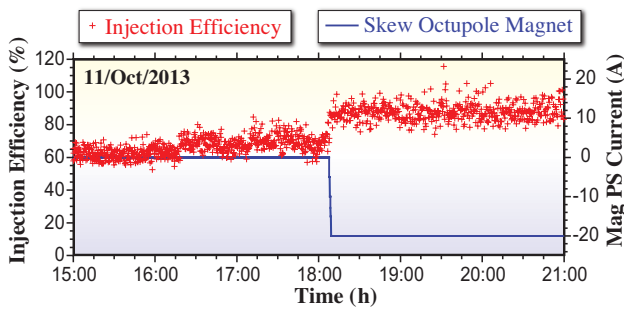


Fig. 3. Trend of the injection efficiency and the exciting current of the skew octupole magnet.

### Upgrade of the Bunch Purity Monitor

The bunch purity monitor installed at the beam diagnostics beamline I (BL38B2) has been upgraded by introducing the fast time measurement system that employs a time to digital convertor (TDC; V1290N, CAEN) [2] and a hybrid photodetector (HPD; R7110UMOD, Hamamatsu) to detect photons with a high count rate.

HPD is a type of photomultiplier tube that incorporates a photocathode and an avalanche photodiode (APD) in an evacuated electron tube. In the HPD, a high electric field applied to the photocathode accelerates the photoelectrons emitted from the photocathode. These photoelectrons are bombarded onto the APD and deposit their kinetic energy in the APD to generate electron-hole pairs (electron bombardment gain). The secondary

electrons are collected and further multiplied by the avalanche gain in the APD. These effects realize a total gain of  $10^4$  or higher, which is sufficient to detect single photons. Additionally, the R7110U series HPD has a sufficient time resolution to discriminate a bucket separation of 2 ns.

V1290N is a 16 ch, high performance multi-hit TDC with a time resolution of 25 ps and a double hit resolution of 5 ns. It has a full-scale range of 52  $\mu$ s, which is sufficient to measure the whole 4.8  $\mu$ s revolution period of the electron beam. An output signal of the HPD of about 500 kcps and a reference-timing signal, which is synchronized to the revolution of the electron beam (208.8 kHz), are fed into two of the TDC channels. The time difference between two signals is processed statistically by software controlling the TDC.

Development of the software, setup of the HPD and other hardware devices were completed in November 2013, and upgraded bunch purity monitor is operational. The result of a 20-min bunch purity measurement is shown in Fig. 4. The high count-rate detection of the HPD and high speed signal processing capacity of the TDC allow the bunch impurity to be evaluated on the  $10^{-9}$  order within 20 seconds and enable an immediate bunch purity measurement of a topped up bunch at every top-up injection.

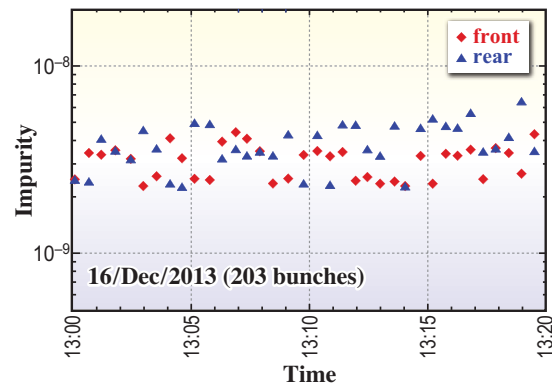


Fig. 4. Result of the bunch purity measurement. Measurements are successfully repeated at intervals of about 30 s after every topping-up injection.

### Development of X-ray Fresnel Diffractometry to Measure the Light Source Size of Insertion Devices

A novel technique using X-ray Fresnel Diffractometry (XFD) has been developed to measure the micron electron beam size at a source point of an ID. An ID source size measurement using XFD

enables us to evaluate the brilliance of undulator radiation at each beamline. XFD uses monochromatic X-ray Fresnel diffraction via a single slit with an optimized width to create a double-lobed diffraction pattern as shown in Fig. 5. The principle is based on the correlation between the depth of the median dip in the double-lobed pattern and the source size at the ID; that is, the valley of the dip becomes shallower as the source size increases. XFD can be positioned as an evolutionary form of a conventional X-ray pinhole camera (XPC) because using monochromatic X-ray and optimizing the pinhole size improves the XPC resolution. XFD has the potential to measure a very small electron beam size less than 1  $\mu\text{m}$  (r.m.s.) when the slit is placed a short distance (several meters) from the source point and the observing X-ray energy is several tens of keV. Therefore, the XFD should be useful for ultra-low emittance diagnostics of next generation light sources such as a diffraction limited storage ring.

A vertical source size measurement using XFD was demonstrated at the beam diagnostics beamline II (BL05SS)[3] with an ID (ID05) [4]. An undulator radiation of 7.2 keV was diffracted by a front-end 4-jaw slit with an optimized vertical width of 150  $\mu\text{m}$  and a horizontal width of 200  $\mu\text{m}$ . The Fresnel diffraction pattern was observed using a high-resolution X-ray imaging apparatus called beam monitor (HAMAMATSU) placed 65.4 m from the slit. Figure 6 shows the observed diffraction images at four operation points with different horizontal betatron tunes with and without skew quadrupole magnets for betatron coupling correction. The double-lobed structures are clearly observed in the vertical direction, but are smeared in the horizontal direction due to large horizontal emittance. The reduction in the contrast of the double-lobed patterns indicates growth of the vertical electron beam size at the ID05 source point due to the increased betatron coupling.

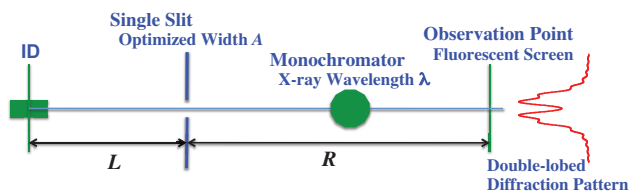


Fig. 5. Layout for the source size measurement of ID using X-ray Fresnel diffractometry.

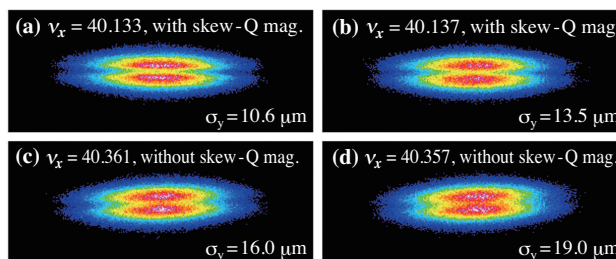


Fig. 6. Double-lobed Fresnel diffraction images observed at four operation points with different horizontal betatron tunes  $\nu_x$ . Vertical betatron tune  $\nu_y$  is fixed at 19.35. Image (a) and other three images (b), (c), (d) are observed with and without skew quadrupole magnets, respectively. Vertical beam sizes are evaluated from the depths of the median dips in the vertical line profiles.

### Development of Ultra-fast Variable Field Kicker for Bucket-by-bucket Beam Handling

For the bucket-by-bucket handling of the multi-GeV beam in a few nano-second timescale, a variable field ultra-fast kicker has been proposed and developed [5,6]. The kicker is a TEM mode stripline type and the kick field distribution is continuously variable from a dipole to a quadrupole by changing the drive voltage of the two stripline electrodes as shown in Fig. 7. To realize a short kick duration of  $\sim 4$  ns for 2 ns spacing bucket, the stripline is set to 0.2 m.

The quadrupole kick can be applied to an off-axis injection into the storage ring with a very narrow dynamic aperture of few mm, like future light sources, with smallest perturbation on stored beam. The dipole kick is for an on-axis swap injection ring with a much narrower dynamic aperture and enables 100-mA average current operations by bucket-by-bucket base handling. Although fast dipole kickers with horizontally separated parallel plates have been proposed for damping rings for linear colliders, their narrower apertures causes issues with synchrotron radiation irradiation. On the other hand, our kicker has an unlimited horizontal aperture with a high and flat

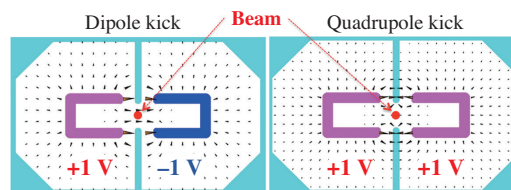


Fig. 7. Cross sectional view of kicker electrode and electric field. (a) Dipole kick field driven opposite polarity pulses for left and right stripline electrodes. (b) Quadrupole kick driven by the same polarity pulses.

dipole kick field distribution, which is one advantage compared to parallel plate types.

The beam test of the kicker was performed with a 1-GeV electron beam from the SPring-8 linear accelerator. The kick strength and the beam profile of the kicked beam were measured with two Ce:YAG screen beam profile monitors installed just after the kicker and its 8 m downstream. To measure the kick field distribution, the kicker was mounted on a horizontally and vertically movable stage. At the beam test, just one electrode of the kicker was driven by a +50 kV 2 ns pulse generator. The time structure of the kick was measured by changing the timing between the kick pulse and the electron bunch (Fig. 8). The maximum kick angle is 0.6 m-rad, which is comparable to designed value that includes the cable loss of the kick voltage.

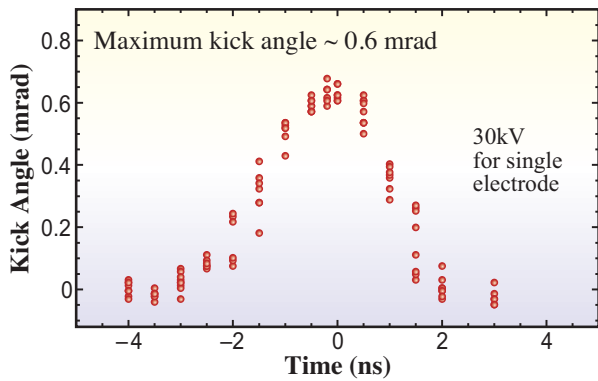


Fig. 8. Time structure of the kick. Maximum kick angle is 0.6 m-rad, which corresponds to 30 kV pulse, but degrades with the cable loss from the maximum available voltage of 40 kV at the pulse generator.

### Improvement of Data Acquisition Scheme in the COD Measurement System

The beam position acquisition scheme was modified for the closed orbit distortion (COD) measurement system. The system modification effectively identifies the beam abort source during the user operation in some cases.

An interlock system is in operation which turns off RF acceleration signals and leads to beam abort when the beam orbits at the insertion devices exceed the pre-defined window. Although rare, beam abort events occurred several times in 2012 and 2013; in most cases problems originated from the source of the beam orbit shift the accelerator devices, but the cause could not be identified when the source of the orbit shift was restored by itself in short time. Thus, we have developed a scheme to modify the existing

COD measurement system, which has been operating since 2008, to observe the beam orbit shift along the storage ring just prior to beam abort.

In the COD measuring system, beam position monitor (BPM) signals are switched sequentially and detected by ADC. A digital signal processor (DSP: Texas-Instruments C6713) controls the COD measurement scheme. There are 48 DSP throughout the ring, which are operated in parallel and roughly synchronized. Before the modification, it took about 15 ms to process all the BPM data by switching every BPM signal, this was too long to obtain the beam orbit just before the beam abort. Moreover, the DSP became idle after the COD measurement was finished until the supervising computer, which calculated the orbit correction parameters for the steering magnets, issued the next measurement command.

We shortened the switching time from 1 ms to 70  $\mu$ s. Moreover, we made DSP not to enter an idle state. As a result, all the BPM positions are recorded every 1 ms in a ring buffer on the DSP board. When the stored beam is lost by the interlock system, the DSP detects a voltage drop in the BPM sum signal and stops the ring buffering update.

We can identify the source of beam orbit shift by analyzing the ring buffer data. Figure 9 shows the orbit shift obtained by the modified system when the beam is aborted by the interlock system. A particular COD pattern grows in 10 ms and the beam is lost. Figure 10 shows the analysis of the closed orbit correction just before the beam is lost. In this case, one of the steering magnets is the source of the beam orbit shift.

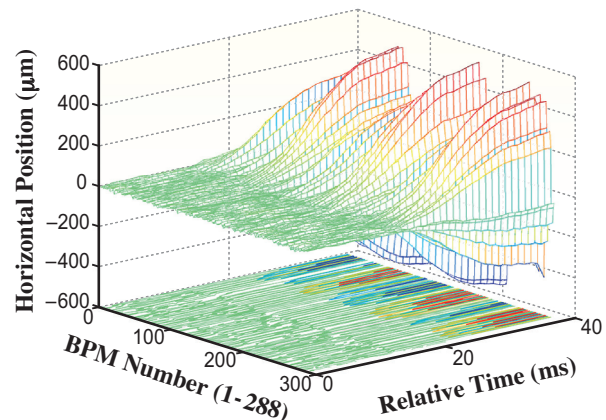


Fig. 9. Horizontal closed orbit grows more than 500  $\mu$ m in 10 ms, and the beam is aborted by the interlock system. Closed orbit data is stored every 1 ms and used for the beam orbit shift analysis.

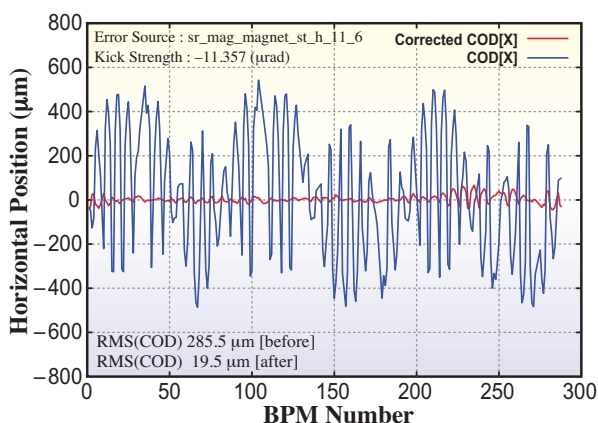


Fig. 10. Analysis of closed orbit just before beam is aborted. In this case, the steering magnet is the orbit shift source.

### Suppression of Stored Beam Oscillation during Injection by Fast Kickers in the SPring-8 Storage Ring

The residual oscillations during injection to the storage ring are suppressed more significantly than before by adding a correction kicker magnet in 2013. The suppression of light axis oscillation was confirmed with TTPM (turn by turn beam profile monitor) [7].

Four pulsed bump magnets are used for injection into the storage ring. There are residual oscillations of the stored beam orbit due to imperfections of bump magnet pulse shape matching, such as timing jitters between the four pulses, pulse shape difference of the rising and falling part of the half sine pulses of 8- $\mu$ s width, etc. The magnitude of amplitude oscillation is 0.4 mm (r.m.s.), but there are 400~700 ns wide spike-like oscillations due to at rising part mismatch and 0.25-mm amplitude with 1.4- $\mu$ s width due to the falling part mismatch.

We started studies to suppress the residual oscillations using a correction kicker in 2010 [8,9]. The correction has been applied during user time since 2012 to suppress the spike-like oscillations due to the rising part mismatch. In 2013, an additional correction kicker was installed to suppress the broader part, due to the falling part.

We tuned the correction kickers by observing the suppression effect with SPBPM (single pass BPM). Figure 11 compares the oscillation amplitude with and without the correction observed with SPBPM, the horizontal axis is the turn number where zero indicates the injection time. The spike-like oscillation amplitude of 0.45 mm (r.m.s.) at the third turn is reduced by 90%. By adding the second correction kicker, the averaged oscillation amplitude is suppressed to a level less than 0.15 mm within fifth revolution of the stored beam.

Since light axis oscillation suppression is necessary from the viewpoint of synchrotron radiation usage, we confirmed that the light axis oscillation is suppressed with TTPM, which measures the monochromatic light beam profile of the insertion device radiation at the beam diagnostic beamline (Fig. 12). A huge light axis oscillation is generated and the data is saturated over the detection range up to the third turn after the injection. After applying the fast correction kicker at the third turn, the oscillation is reduced at least by 87%, down to 4  $\mu$ rad. Without the kicker correction, it takes about 80 turns to reduce the oscillation, which was determined by the damping time with the bunch by bunch feedback system [10].

All data acquired by the SPBPM and TTPM system show a consistent result for the suppression effect. It is concluded that the residual oscillation in the horizontal direction at injection is reduced by a factor of five, within the fourth turn after injection by applying the correction scheme with the two kicker systems.

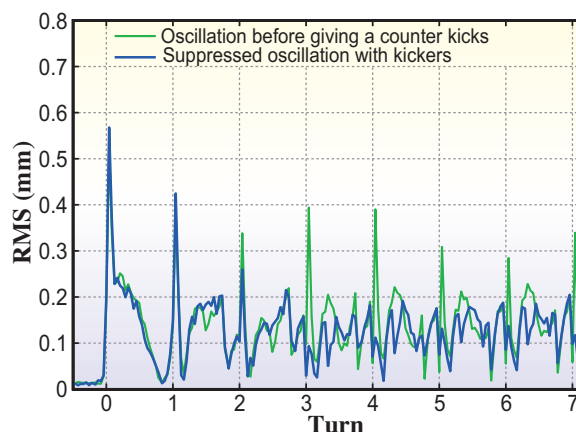


Fig. 11. R.M.S. values of the residual oscillation vs turn number after injection, where 0 corresponds to the injection time. Counter kick is applied at third and fourth turns for the primary and secondary kicker, respectively.

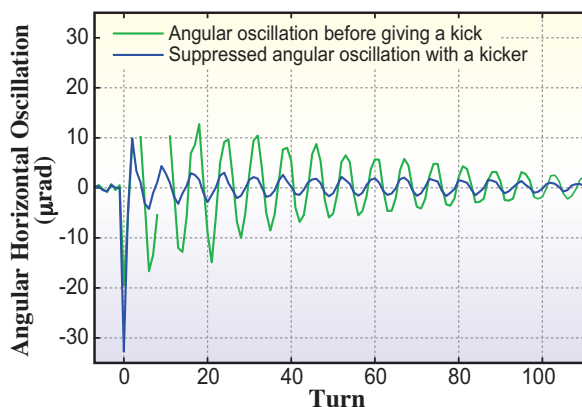


Fig. 12. Angular horizontal oscillation observed by TTPM. Oscillation data under 10 turns is saturated because the oscillation amplitude is more than 30  $\mu$ rad.

### Prototype Circuit using FPGA for Trigger Timing System in SPRing-8 Linac

To easily setup a high-speed logic system, NIM modules are common in timing system for the injector linac. However, the large number of modules (more than 100) make it difficult to modify the timing system because the hundreds of cables outside already connect the modules and there is no more space to install additional modules for further improvements.

To fundamentally solve this problem, we have developed and tested a prototype circuit using an field-programmable gate array (FPGA). An FPGA is an LSI that we can reprogram to compose a complicated logic circuit. The prototype system is much smaller, and should have a higher functionality and reliability than the current complex system.

For the prototype, we adopted a Vertex-6 FPGA ML623 Characterization Kit produced by Xilinx as an FPGA board (Fig. 13). Re-clocking circuits were added to all output ports of the FPGA board to minimize the timing jitters.

In one FPGA, we create a program, which include half of the current timing system. This prototype circuit functions properly and results in output signals

with jitters less than 2.5 ps, which is sufficient for electron gun trigger signals. However, the number of counter delay circuits in FPGA must be less than four at a clock frequency of 508 MHz due to the signal delay time, which limits the scale of the circuit in the FPGA. Thus, three PFGAs are necessary to replace all the current timing system. The prototype will be modified to replace the modulator trigger system, while another larger circuit with two or three FPGAs will be developed to replace all others in the future.

Haruo Ohkuma\*, Shigeki Sasaki and Hirofumi Hanaki  
 SPRing-8/JASRI

\*E-mail: ohkuma@spring8.or.jp



Fig. 13. Prototype of the trigger timing circuit with an FPGA. It has 50 NIM inputs, 50 NIM outputs, and 3 clock inputs. Half of the current timing system is programmed in the FPGA.

#### References

- [1] T. Tanaka and H. Kitamura: SPECTRA code ver. 9.02 (2012).
- [2] A. Kiyomichi *et al.*: Proc. 9th Annual Meeting of Particle Accelerator Society of Japan, Osaka, Japan, 2012, p. 701 (in Japanese).
- [3] S. Takano *et al.*: Proc. IBIC2012, Tsukuba, Japan, p.186.
- [4] M. Masaki *et al.*: AIP Conf. Proc. **1234** (2010) 560.
- [5] T. Nakamura: Proc. IPAC '11, San Sebastian, Spain, p.1230.
- [6] T. Nakamura *et al.*: Proc. 9th Annual Meeting of Particle Accelerator Society of Japan, Osaka, Japan, 2012, p. 525 (in Japanese).
- [7] M. Masaki *et al.*: Proc. IBIC2012, Tsukuba, Japan, 2012, p.492.
- [8] C. Mitsuda *et al.*: Proc. IPAC'10, Kyoto, Japan, 2010, p.2252.
- [9] C. Mitsuda *et al.*: Proc. of IPAC'13, Shanghai, China, 2013, p.666.
- [10] T. Nakamura *et al.*: Proc. of IPAC'11, San Sebastian, Spain, 2011, p.493.